Research Article | Vol. 9, No. 9 / 1 September 2019 / Optical Materials Express 3582
Optical Materials EXPRESS

Femtosecond laser ablation and photo-induced effects of $As_{40}S_{60}$, $Ga_{0.8}As_{39.2}S_{60}$ and $Ga_{0.8}As_{29.2}Sb_{10}S_{60}$ chalcogenide glasses

Lutao Liu,[1,2] Xin Zheng,[2,3] Xusheng Xiao,[1] Yantao Xu,[1,2] Xiaoxia Cui,[1,2] Jian Cui,[1,2] Chunlei Guo,[3,4] Jianjun Yang,[3,5] and Haitao Guo[1,2,6]

[1] *State Key Laboratory of Transient Optics and Photonics, Xi'an Institute of Optics and Precision Mechanics, Chinese Academy of Sciences (CAS), Xi'an, Shaanxi 710119, China*
[2] *Center of Materials Science and Optoelectronics Engineering, University of Chinese Academy of Sciences (UCAS), Beijing 100049, China*
[3] *The Guo China-US Photonics Laboratory, State Key Laboratory of Applied Optics, Changchun Institute of Optics, Fine Mechanics and Physics, Chinese Academy of Sciences (CAS), Changchun Jilin 130033, China*
[4] *The Institute of Optics, University of Rochester, Rochester, NY 14627, USA*
[5] *jjyang@ciomp.ac.cn*
[6] *guoht_001@opt.ac.cn*

Abstract: Laser induced damage thresholds (LIDTs) and photo-induced changes of $As_{40}S_{60}$, $Ga_{0.8}As_{39.2}S_{60}$ and $Ga_{0.8}As_{29.2}Sb_{10}S_{60}$ chalcogenide glasses are investigated by femtosecond laser of 800 nm. $As_{40}S_{60}$ glass has the highest LIDT as well as 1452.3 mJ/cm^2, the introduction of small amount of Ga and Sb into glass decreases the LIDTs to 957.1 mJ/cm^2 for $Ga_{0.8}As_{39.2}S_{60}$ and 705.9 mJ/cm^2 for $Ga_{0.8}As_{29.2}Sb_{10}S_{60}$, respectively. Microstructure analysis reveals that the decrease of LIDT is tightly related to the decrease of high strength chemical bonds and formation of lower ones in glass matrix. After multi pulses induced damage occurred, the structure of glass matrix became more random and a half of S was replaced by O approximately. The damage mechanism was proposed and it is helpful to develop high LIDT chalcogenide glasses and the photo-induced effects are the basis of waveguide writing in chalcogenide glasses by femtosecond laser.

1. Introduction

Chalcogenide glass (ChG) refers to a kind of glass based on chalcogen elements (sulfur, selenium and tellurium) combined with group III-V elements [1]. Because of some attractive optical properties including low phonon energy [2], high linear and nonlinear refractive index [3], ChG is one of the most important infrared (IR) optical materials to be made into IR lens or waveguides like fibers which can be applied in IR sensing and imaging [4]. Besides the passive optical applications, it can also be doped with rare-earth (RE) elements to become promising gain materials for mid-IR lasers and fiber-optic amplifiers which have potential applications in the medical field, national defense and remote sensing [5].

Among various ChGs, $As_{40}S_{60}$ glass is the first kind of ones which is brought out in 1950 [6]. Since its birth, it has attracted much attention mainly because it can be made into low loss IR fibers [7]. However, it shows low solubility of RE ions which limits its application in active devices like gain media in IR lasers or amplifiers [8]. Luckily, its properties are tunable through compositional tailor. Other elements, such as Ga, Sb and Ge can be introduced into it to change the microstructure of As-S glass to improve its properties. For example, the replacement of As by a little Ga can improve the solubility of RE ions in glass matrix prominently [9,10]. Jian Cui et al. prepared a serial different concentration Dy^{3+} doped $Ga_{0.8}As_{39.2}S_{60}$ glasses and found that the

#370767 https://doi.org/10.1364/OME.9.003582
Journal © 2019 Received 24 Jun 2019; revised 25 Jul 2019; accepted 27 Jul 2019; published 2 Aug 2019

Optical Materials EXPRESS

$Ga_{0.8}As_{39.2}S_{60}$ glass has much higher solubility of RE ions than that of $As_{40}S_{60}$ and more than 3000 ppm Dy^{3+} ions can be doped in the $Ga_{0.8}As_{39.2}S_{60}$ glass for fiber drawing [11]. However, the Ga-As-S system shows a small glass formation region. Some amount of Sb can improve the fiber drawing performance to neutralize the impact of Ga [12].

For Ga-As-S, Ga-As-Sb-S novel ChGs and fibers, their optical, mechanical and thermal properties are very important and have been investigated in former works, while other important properties, laser induced damage threshold (LIDT) and photo-induced effects, should also be studied for further applications.

During the last two decades, LIDT or photo-induced effects of several kinds of ChGs or fibers were investigated, including As-S/Se [13,14], Ge-S [15], Ge-Sb-S/Se [16,17], As-Sb-S [18], Ge-As-S [19,20]. The damage process can be divided into three steps including energy deposition, initial material response and damage signature [21]. Change of glass composition can influence all the three steps. For instance, the addition of Se into As-S glass can decrease the band gap and then the degree of multiphoton absorption becomes low which contributes to the decrease of LIDT in As-S-Se glass [14]. Different glasses have different composition of chemical bonds, some may have higher strength to others, which means different energy is needed to break them, and it influences the second part.

Nowadays, the time resolution of detection to femtosecond laser ablation is not as fast as the laser pulse, so the influence of material composition to LIDT is mainly analyzed by postmortem. On the other hand, there are so many factors like laser repetition rate, pulse duration and beam focus influencing the damage results. Different researchers present different damage mechanism such as cold ablation [20], heat accumulation [22] and mixture of the two mechanisms [14].

As a potential material to be used as mid-infrared waveguide or active devices, its capacity for high power laser transmission needs to be considered when applied on certain devices. Besides, direct laser writing in ChG fiber to make Bragg fiber grating (FBG) needs photo-response properties which include photon-induced index changes and LIDT [23,24]. Highly refractive and low-loss FBG plays a key role in efficient IR fiber laser. Therefore in this work, laser ablation property of As-S glass family including $As_{40}S_{60}$, $Ga_{0.8}As_{39.2}S_{60}$ and $Ga_{0.8}As_{29.2}Sb_{10}S_{60}$ are studied systematically. We explored the effect of introduction of Ga and Sb to the LIDT of $As_{40}S_{60}$ glass and explained it by Raman spectrometer and UV-VIS-NIR transmission spectrometer. In addition, the effects of femtosecond laser radiation to all these three glasses were investigated by SEM&EDS and Raman spectrometer. According to the results, the process of laser damage was speculated.

2. Experiment

$As_{40}S_{60}$, $Ga_{0.8}As_{39.2}S_{60}$ and $Ga_{0.8}As_{29.2}Sb_{10}S_{60}$ bulk samples were prepared by the conventional melt-quenching technique. Raw materials include Ga (7N, grains, Aladdin Industrial Co. Ltd. China), As (5N, grains, Mount Emei Jiamei High Pure Material Co. Ltd. China), Sb (6N, grains, SCRC Co. Ltd., China), S (6N, powders, SCRC Co. Ltd. China). All the raw materials were weighed in the glove-box using an analytical balance (Sartorius) whose resolution is 0.001 g. Then the weighed materials were transferred into a clean ampoule and the ampoule was sealed under vacuum (10^{-4} Pa). After that, the ampoule was put into a rocket furnace to be heated for 12 hours ($As_{40}S_{60}$: 650 °C, $Ga_{0.8}As_{39.2}S_{60}$: 950 °C, $Ga_{0.8}As_{29.2}Sb_{10}S_{60}$: 950 °C). Once times up, the melt was quenched in water and then annealed ($As_{40}S_{60}$: 180 °C, $Ga_{0.8}As_{39.2}S_{60}$: 185 °C, $Ga_{0.8}As_{29.2}Sb_{10}S_{60}$: 185 °C). Finally, the glass rod was sliced and polished to mirror smoothness with a thickness of 5.0 mm for the damage experiments.

We used a chirped pulse regenerative Ti: sapphire laser amplifier system (Spitfire Ace, Spectra Physics) to generate linearly polarized laser pulses with a pulse duration of 40 fs and a central wavelength of 800 nm at a pulse repetition of 1 kHz. A half-wave plate cooperating with a Glan-Taylor prism was used to control the laser energy which can be measured by a pyro-electric

Optical Materials EXPRESS

detector (3A-PF-12, Ophir). In order to achieve the damage ablation, the laser pulses were focused onto the sample surface at normal incidence by an objective lens (4×, NA = 0.1) and the full width at half maximum (FWHM) intensity of focused laser beam is 6.62 μm based on calculation. For obtaining the single-pulse ablated crater, the samples were mounted on a computer-controlled three dimensional translation stage (M-ILS100HA, Newport) and translate with a velocity of 50 mm/s. All damage experiments were conducted in the air. The experiment setup is illustrated in Fig. 1.

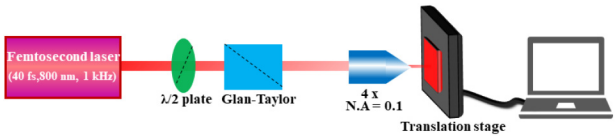

Fig. 1. Illustration of the damage experiment setup

The morphology of damaged spots were observed by optical microscope (Olympus BX53M) whose maximum magnification is 1000X and field emission scanning electron microscope (Zeiss Gemini SEM 500) whose resolution is 0.6 nm at 15 kV. The absorption spectra were measured by a JASCO V-570 UV-VIS-NIR spectrophotometer from 500 to 1000 nm with the spectral step of 2 nm. The microstructure of unexposed region and laser damaged region were characterized by Laser Raman Spectrometer (LabRAM HR Evolution) whose resolution is 0.35-0.65 cm^{-1}. Samples were excited by a 785 nm NIR diode laser at an incident power of 0.5 mW and acquisition time of 30 s. The low excitation power and long acquisition time in the characterization is to avoid photo-structure changes during the illumination of excitation laser. In order to detect a micro region on the surface of sample where damage occurred, a 100X objective was used to focus the excitation laser. Detected range is from 150 cm^{-1} to 600 cm^{-1}. The smoothing, baseline subtraction, peak finding and peak fitting of Raman spectra were performed on Origin Pro 2017 software. The element variation before and after laser damage was characterized by energy dispersive spectrometer (EDS) equipped on FE-SEM when SEM images are taken. All measurements were performed at room temperature.

3. Results and discussion

3.1. Morphology analysis

Figure 2 shows the morphology of damaged spots which look like craters. All damaged craters on the surfaces of $As_{40}S_{60}$, $Ga_{0.8}As_{39.2}S_{60}$ and $Ga_{0.8}As_{29.2}Sb_{10}S_{60}$ show three features. Firstly, craters grow broader with the increase of incident laser power and even become bigger than the FWHM of incident laser beam. Secondly, when the incident laser power get bigger the damaged crater becomes more symmetric. As seen in the last crater of $As_{40}S_{60}$, when laser power increases to 20.1 mW, the corresponding crater looks like a perfect circle. Lastly, circled regular ripples appear at the rim of crater when the incident laser power is high enough.

As for the first feature, the incident laser is Gaussian beam, which can be described as follow [25]:

$$I(r,\ t) = I_0 \exp(-\frac{r^2}{\rho^2}) \exp(-\frac{t^2}{\tau^2}) \tag{1}$$

where I_0 is the peak intensity, ρ and τ are spatial and temporal radius respectively. Then, the spatial energy distribution of a Gaussian laser beam can be integrated by time:

$$F(r) = \int_{-\infty}^{\infty} dt I(r,\ t) = F_0 \exp(-\frac{r^2}{\rho^2}) \tag{2}$$

Optical Materials EXPRESS

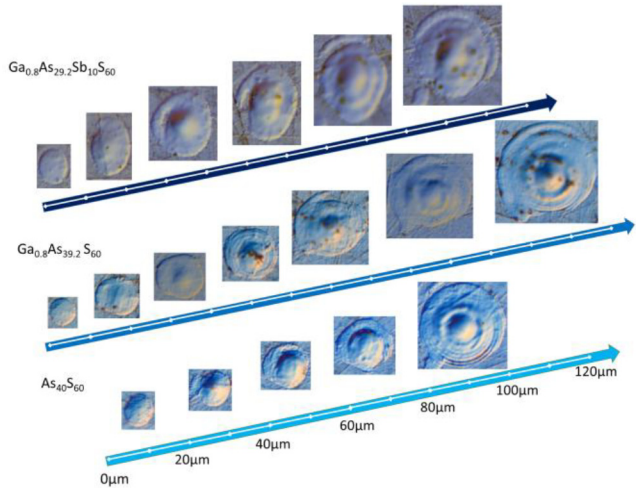

Fig. 2. Morphology of damaged spots on $As_{40}S_{60}$ (bottom), $Ga_{0.8}As_{39.2}S_{60}$ (middle) and $Ga_{0.8}As_{29.2}Sb_{10}S_{60}$ (top). Laser fluence increases from the tail to the head of the arrow in each group.

where $F_0 = \sqrt{\pi}\tau I_0$ is the max laser fluence at the center of beam. Once the fluence $F(r)$ exceeds the laser induced damage threshold (LIDT) F_{th}, damaged crater occurs:

$$F(r_{th}) = F_0 \exp(-\frac{{r_{th}}^2}{\rho^2}) = F_{th} \tag{3}$$

where r_{th} is the radius of damaged crater. From Eq. (3), we can see clearly that even the r_{th} is bigger than ρ, F_{th} can still be reached. It means that the ρ (which means FWHM of laser beam) is not the limit of radius of damaged craters. Besides, we can extract r_{th} out of Eq. (3):

$${r_{th}}^2 = \rho^2(\ln F_0 - \ln F_{th}) \tag{4}$$

According to the Eq. (4), we can not only understand how the radius of damaged craters grow with the increase of incident laser power but also get the LIDT by linear fit of ${r_{th}}^2$ to $\ln F_0$. The LIDT and linear fit will be showed later.

The second feature is due to a "self-healing" effect of high intensity laser pulse. The output beam is inevitable to be affected by astigmatism and beam divergence, which account for the asymmetry of incident laser beam and correspondent elliptical damaged crater. While at high laser fluence, laser ionized air before reaching the surface of glass. The ionized air flattened laser beam to be more symmetric, which looks like high intensity laser heals itself [26,27].

The last feature may be due to the interference of laser beam when passing through the focusing lens which is known as "Newton's ring". We measured the radius of homocentric ripples, and find out that the ratio of outer ripple to the first ripple at center is very similar to a change regulation of $\sqrt{n}$, which is in accordance with the radius of Newton's ring of $\sqrt{kR\lambda}$, in which k is a constant (1,2,3, etc.), R is the refractive index and λ is the wavelength. All the radius, ratio of ripple and ratio of Newton's ring with different n are listed in Table 1.

3.2. LIDT of 3 different glasses and impacts of LIDT

Figure 3 shows the linear fit of Eq. (4), from which we can find that the highest LIDT belongs to $As_{40}S_{60}$ as well as 1452.3mJ/cm^2, and it decreases to 957.1 mJ/cm^2 when 0.8% of Ga is added, and further decreases to 705.9 mJ/cm^2 for $Ga_{0.8}As_{29.2}Sb_{10}S_{60}$.

Optical Materials EXPRESS

Table 1. Compare of homocentric ripples' radius to Newton's ring

Radius and Ratio	1	2	3	4	5	6
Radius of ripple (μm)	4	5.6	6.8	7.8	8.8	9.6
Ratio to the first ripple	1	1.40	1.70	1.95	2.20	2.40
Ratio of Newton's ring $=\sqrt{n}$	1	1.41	1.73	2.00	2.24	2.45

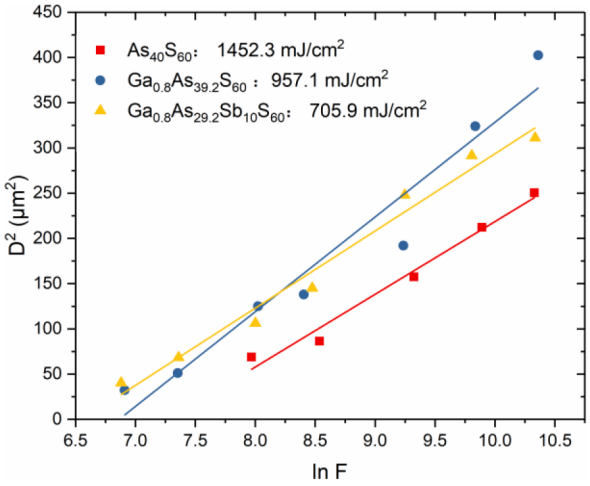

Fig. 3. Linear fit of LIDT of $As_{40}S_{60}$, $Ga_{0.8}As_{39.2}S_{60}$ and $Ga_{0.8}As_{34.5}Sb_5S_{60}$

To understand what are responsible for this decreasing trend, UV-VIS-NIR transmission spectrometer and micro-Raman spectrometer are carried out. Figure 4(A) shows the absorption spectra of three glasses in the UV-VIS-NIR region, from which we can find that all the absorption at 800 nm are almost 0 cm^{-1}. Figure 4(B) is the linear fit to calculate band gap based on the Tauc's equation about band gap of amorphous semiconductors and the interception of fitted dot line to X axis represents corresponding band gap [28]. The band gap of $As_{40}S_{60}$, $Ga_{0.8}As_{39.2}S_{60}$ and $Ga_{0.8}As_{29.2}Sb_{10}S_{60}$ are 2.15 eV, 1.88 eV and 1.94 eV respectively. The photon energy of light at 800 nm is 1.55 eV which is lower than all the band gap of these three glasses. There's almost no absorption at 800 nm because the photon of 800 nm does not have enough energy to excite an electron in the glasses from the valence to the conduction band. But when the intensity of incident laser is high enough, nonlinear absorption occurs such as multiphoton ionization and tunneling ionization. According to the Keldysh's theory [29], multiphoton ionization plays a key role in the case of this damage experiment. All the glasses need at least two photons to be ionized. The absorption rate and degree of multiphoton ionization of the three glasses are almost the same, so the energy absorptions from laser are similar for the three glasses.

Unexposed and exposed region on the surfaces of $As_{40}S_{60}$, $Ga_{0.8}As_{39.2}S_{60}$ and $Ga_{0.8}As_{34.8}Sb_5S_{60}$ were all detected by micro-Raman spectrometer for verifying the microstructure's changes before and after the laser irradiation.

Figure 5 shows the Raman spectra of as prepared $As_{40}S_{60}$, $Ga_{0.8}As_{39.2}S_{60}$ and $Ga_{0.8}As_{29.2}Sb_{10}S_{60}$. The spectra are decomposed into several Gaussian peaks that correspond to different structural units. Red line (sum of decomposed peaks) is in good accordance with dot line (the original Raman spectra). The broad band in the Raman spectrum of $As_{40}S_{60}$ consists of four peaks such as asymmetric stretching of $AsS_{3/2}$ network units whose Raman peak is centered at 310 cm^{-1} [30], symmetric stretching of $AsS_{3/2}$ whose Raman peak is centered at 345 cm^{-1} [30], A_1 breathing motion of As_4S_4 whose Raman peak centered at 365 cm^{-1} [31] and T_2 stretching motion of

Optical Materials EXPRESS

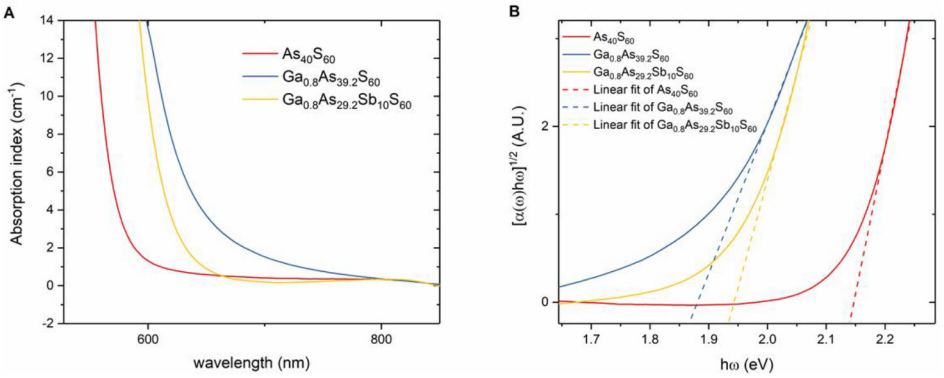

Fig. 4. Absorption spectra (A) and linear fit of band gap (B) of $As_{40}S_{60}$, $Ga_{0.8}As_{39.2}S_{60}$ and $Ga_{0.8}As_{34.8}Sb_5S_{60}$

$S_{2/2}$As-S-As$S_{2/2}$ network bridges whose Raman peak is centered at 380 cm^{-1} [30]. Besides, there are three small peaks locating out of the broad band. They are B_1 stretching mode of As_4S_4 molecule whose Raman peak is centered at 210 cm^{-1} [31], stretching of S2/2As-AsS2/2 homopolar network bonds whose Raman peak is centered at 235 cm^{-1} [32] and A_1 mode of S-S bond in S_n chains whose Raman peak is centered at 490 cm^{-1} [33].

Introduction of 0.8% Ga changes several bands comparing to those of $As_{40}S_{60}$. A new band centered at 350 cm^{-1} is formed, which represent the symmetric stretching of GaS_4 [34]. Band at around 490 cm^{-1} decreases, it means the decrease of S-S bond of S chain. Besides, bands at 210 cm^{-1} and 365 cm^{-1} decrease while band at 380 cm^{-1} increases. That means the As_4S_4 molecule decreases and the $S_{2/2}$As-S-As$S_{2/2}$ network bridges increases which seems that the As_4S_4 molecule is polymerized into the glass network [18]. Addition of 10% Sb into $Ga_{0.8}As_{39.2}S_{60}$ glass matrix changes its Raman spectra heavily. The main band has a blue shift from 345 cm^{-1} to 325cm^{-1}, besides, band at around 490 cm^{-1} and band at around 235 cm^{-1} both decrease. The blue shift of main band is attributed to the formation of SbS_3 triangular cone structure whose Raman peaks are centered at 290 cm^{-1} and 314 cm^{-1} [35,36]. The same band in different glasses may have a little shift, it may be due to different internal stress in different glasses [37].

Relative amount of different structural units shown in Fig. 5 are derived from the relative ratio of the integrated area of each decomposed peak to that of the whole Raman spectrum. We find that the introduction of Ga and Sb into $As_{40}S_{60}$ glass matrix decreases its LIDT which can be attributed to decomposition of high-strength chemical bonds and formation of low-strength chemical bonds. After the addition of Ga into $As_{40}S_{60}$ glass matrix, As_4S_4 molecules is polymerized into glass network. The As-As chemical bonds may be broken, As-S chemical bonds and As-S-As network bridges become more, where the strength of As-As homopolar bond (382.0 ± 10.5 kJ/mol) [38] is a little higher than that of As-S bond (379.5 ± 6.3 kJ/mol). Besides, some amount of $AsS_{3/2}$ network units are replaced by newly formed GaS_4 network units and S-S bonds almost disappeared after Ga was added. However, As-S chemical bond is stronger than Ga-S bond, and S-S bond (425.3 kJ/mol) in S_n chains is the strongest bond among all the chemical bonds in three glass matrices. After Sb was introduced, the amount of As_4S_4 molecules decreased further and $SbS_{3/2}$ units were newly formed. The bond strength of Sb-S is 378.7 kJ/mol which is a little smaller than that of As-S (379.5 ± 6.3 kJ/mol). To summarize, the decrease of LIDT is in accordance with the decrease of bonds of higher strength and formation of bonds of lower strength when absorption rate of different glasses are similar.

Optical Materials EXPRESS

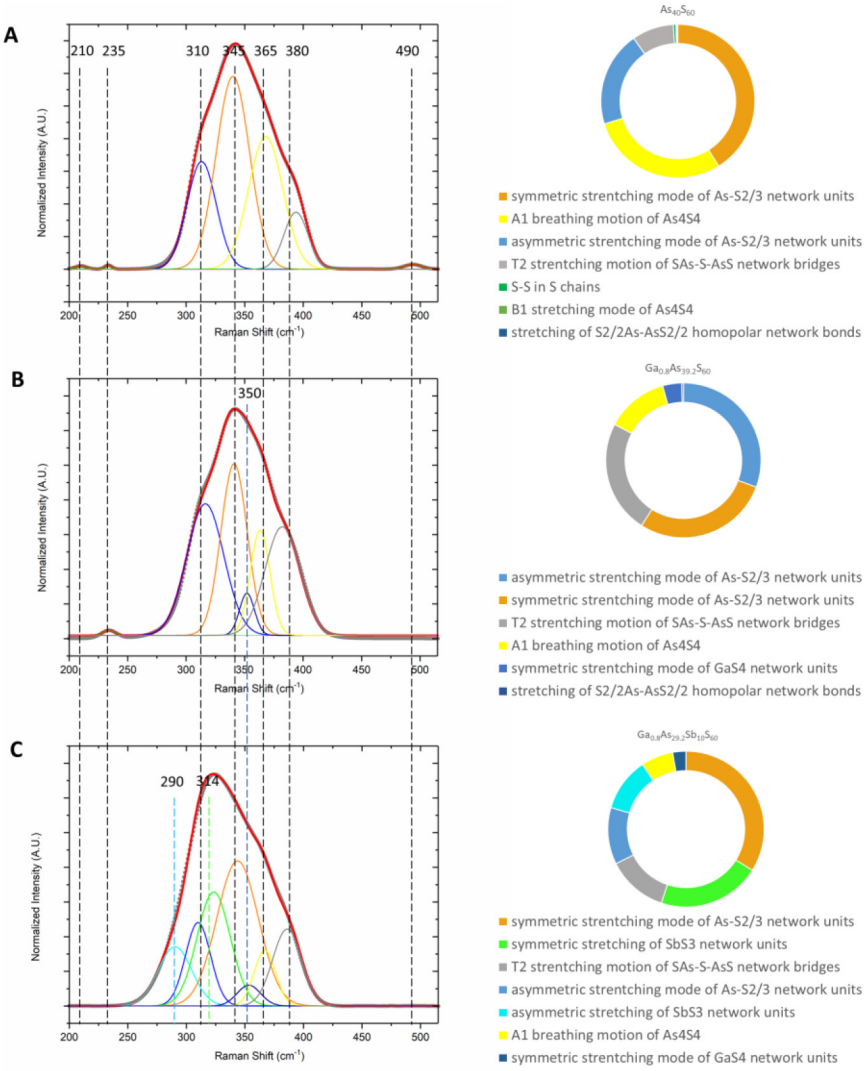

Fig. 5. Decomposition of Raman spectra of $As_{40}S_{60}$ (A), $Ga_{0.8}As_{39.2}S_{60}$ (B) and $Ga_{0.8}As_{29.2}Sb_{10}S_{60}$ (C). The red line is the sum of decomposed peaks and the dot line is the original Raman spectra. The list of different units are sequenced by their relative amounts

LIDT is reached when the excitation pulse has created electron plasma of sufficient energy density in the conduction band to break chemical bonds or heat the matrix to melt [21]. But the femtosecond laser pulse is too short to accumulate enough heat to melt matrix before the energy is high enough to break chemical bonds, because the generated free-electron population need more time to become hot enough for transferring much energy to the lattice than break chemical bonds [27]. C. Schaffer, J. Garćıa, and E. Mazur reviewed the mechanism of femtosecond laser writing and they concluded that in the situation of tightly focused pulses with energy well above the damage threshold, the mechanism is an explosive expansion of the highly energetic electron–ion plasma formed by the laser pulse [39]. In our experiment, an objective lens of NA = 0.4 is used and the pulse energy is definitely above LIDT, which is in accordance with the situation of tightly focused pulses with energy well above the damage threshold. Thus, the average strength of chemical bonds in glass matrix can be a key factor to define LIDT of femtosecond laser if

Optical Materials EXPRESS

absorption rate to the incident laser is similar. The break of chemical bonds can be also confirmed by comparing of Raman spectra and EDS spectra between exposed region and unexposed region on the surfaces of the three glass matrices.

3.3. Photo-induced effects and femtosecond laser damage mechanism

Raman spectrometer and energy dispersive spectroscopy (EDS) results of the single pulse damaged region (SPDR) and unexposed region on all the three glass matrices are almost the same. While all the results of multi pulses damaged region (MPDR) on the three glass matrices show obvious changes to those of unexposed region. The SEM images of different kind of damaged region on the surface of $Ga_{0.8}As_{39.2}S_{60}$ are showed in Fig. 6. The SPDR is shallower than the MPDR whose center became a deep hole. Such a deep hole may make it more difficult for the exciting laser of Raman Spectrometer or the electron beam of EDS to enter, which could make results inaccurate. In order to avoid the effect of deep hole to Raman spectra and results of EDS, all the Raman spectra and EDS results are collected at rim of the damaged craters.

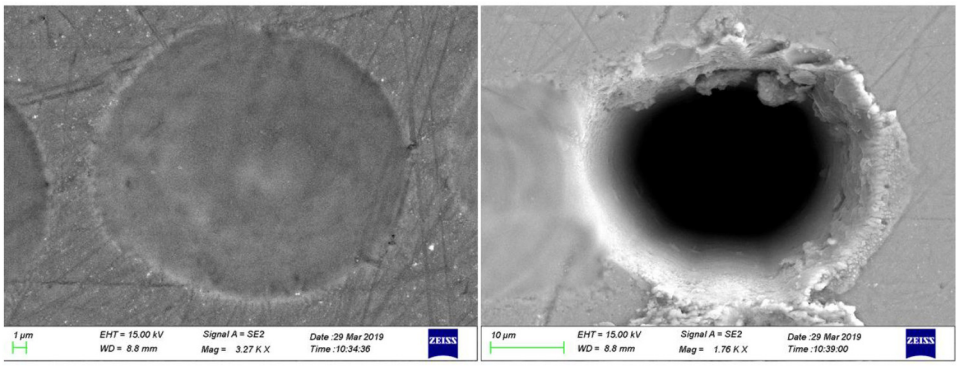

Fig. 6. SEM images of single pulse damaged region (left) and multi pulses damaged region (right) on $Ga_{0.8}As_{39.2}S_{60}$.

The change of a single pulse to the glass matrix is too small to be detected by Raman spectrometer and EDS. Whereas, multi pulses illumination induces enough changes of microstructure and change of elements accumulated on the surface of glass matrix.

In Fig. 7, Raman spectra of MPDR and unexposed region shows that, all the three glass matrices have similar changes after exposed to the incident laser that the amounts of $S_{2/2}$As-As $S_{2/2}$ homopolar network bonds and S-S bonds in S_n chains have increased. This means that the structure of glass matrix became more random after exposure to laser for these are wrong chemical bonds which should not appear in stoichiometric material [40]. The increase of randomness is tightly related to the photo-induced darkening effect [41]. Because the short range order (SRO) changes [42] and electronic states associated with As-As bonds are close to the top of the glass valence band which is preferentially to be excited [43]. And the photo-induced darkening is further related to change of refractive index of glass according to the Kramers–Kronig relations [44,45]:

$$\Delta n(\lambda) = \frac{1}{2\pi^2} \int_0^\infty \frac{\Delta\alpha(\lambda')d\lambda'}{1 - (\frac{\lambda'}{\lambda})^2} \tag{5}$$

where λ is the free space wavelength, $\Delta\alpha(\lambda')$ is the changes of absorption coefficient.

The changes mean femtosecond laser has a huge potential in the field of direct laser writing of waveguide structures on chalcogenide glasses. Efimov el. al. discovered both effects when writing on As-S chalcogenide glasses by a train of femtosecond laser pulses [41]. Besides, the

Optical Materials EXPRESS

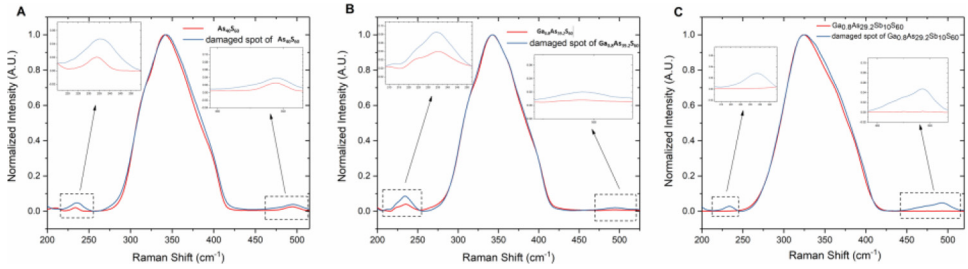

Fig. 7. Structural changes after laser ablation of $As_{40}S_{60}$ (A), $Ga_{0.8}As_{39.2}S_{60}$ (B) and $Ga_{0.8}As_{29.2}Sb_{10}S_{60}$ (C)

homopolar bonds have stronger bond strength than that of the heteropolar bonds in the three glasses [38], more energy is needed to further ablate the damaged spot. It seems that the glass matrix are defending themselves from the damage of femtosecond laser.

Element variation of surfaces for the glass matrices before and after multi laser pulses damage was explored by EDS whose relative measurement error is about ± 1%. In all three glasses, interestingly, about a half of S was replaced by O which was newly introduced into glass matrices after exposure as shown in Fig. 8. The other elements, such as As in $As_{40}S_{60}$ glass and Sb in $Ga_{0.8}As_{29.2}Sb_{10}S_{60}$ glass almost remain the same as before exposure to laser. Ga in $Ga_{0.8}As_{39.2}S_{60}$ and $Ga_{0.8}As_{29.2}Sb_{10}S_{60}$ glasses is not detected because its content is only 0.8% which is beyond the limit of EDS. The trace of O on the surface of unexposed matrix may be from the slow oxidation of glass or the absorption to oxygen because the specimens are reserved in the atmosphere. Besides, The EDS was carried out in the atmosphere, detection of O is inevitable.

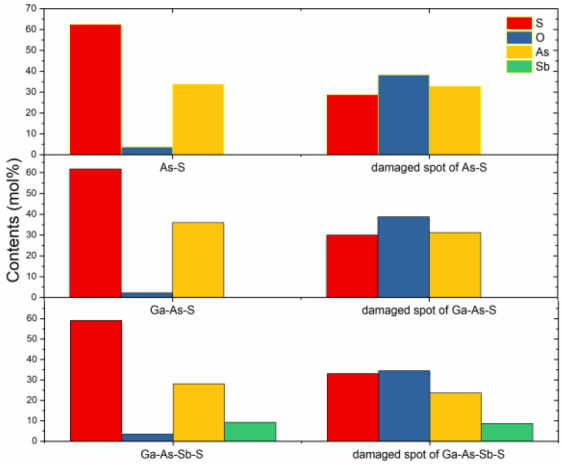

Fig. 8. Element changes after laser ablation of $As_{40}S_{60}$, $Ga_{0.8}As_{39.2}S_{60}$ and $Ga_{0.8}As_{29.2}Sb_{10}S_{60}$

Based on the results, a damage mechanism of femtosecond laser to chalcogenide glasses is proposed, as shown in Fig. 9. Avalanche ionization is confirmed to be the dominant damage mechanism when the repetition rate of femtosecond laser is lower than 1 kHz by M.J. Zhang et.al [20]. Since the photon energy of 800 nm is 1.55 eV which is less than the band gap of all the three chalcogenide glasses, the energy transfer from laser to glass should be in a nonlinear way. Different researchers all noticed significant two-photon absorption in chalcogenide glasses for excitation wavelength in the near infra-red [46,47]. Some valence electrons are excited to

Optical Materials EXPRESS

conduction band by the leading edge of femtosecond laser pulse by two-photon absorption. Then the excited electron plays as the seed electron for avalanche ionization during the rest of the pulse [48]. Electrons in the conduction band are heated by the laser pulse much faster than they can cool by phonon emission. So the electron density grows through avalanche ionization until the plasma frequency approaches the frequency of the incident laser radiation. This is a "critical density", the absorption rate to laser energy reaches the top at this density [49]. Most of the laser energy is transmitted into the matrix so Coulomb explosion occurs [21], which creates plasma plume into the atmosphere. Irimiciuc et. al. photographed plasma plume of chalcogenide glass by fast ICCD imaging [50]. The plasma plume includes several kinds of active ions, such as S^{2-} and As^{3+}. They may interact with oxygen in the atmosphere. Some sulfur become sulfur oxide gases escaping to the atmosphere. Other elements combine with oxygen and still remain in glass matrix. At last, damaged spot occurred and its microstructure and constituent elements changed.

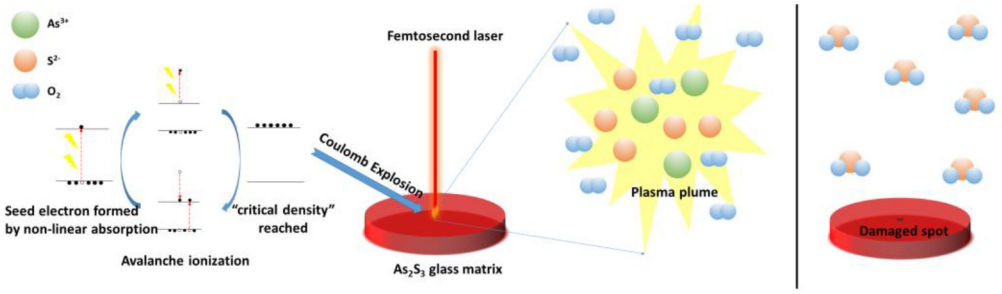

Fig. 9. Illustration of femtosecond laser damage to $As_{40}S_{60}$ glass

4. Conclusion

The addition of Ga and Sb into $As_{40}S_{60}$ decreases the LIDT from 1452.3mJ/cm^2 to 957.1mJ/cm^2 and 705.9mJ/cm^2, because strong chemical bonds like S-S are replaced by weaker chemical bonds like Ga-S and Sb-S, less energy was needed to be absorbed from laser to break them to cause the ablation. Single pulse damage and multi pulses damage show different morphology. After irradiated by multi femtosecond laser pulses, their structure become more random which means As-As and S-S homopolar network bonds increase while they are not supposed to appear in stoichiometric material. Besides, about a half of S in the three glass matrices are replaced by O which are newly introduced after laser irradiation while the other elements almost remain the same as before irradiation. Based on the results, a mechanism of femtosecond laser ablation to chalcogenide glasses is proposed. It may be useful to explore the development of high LIDT chalcogenide glass and provide some theoretical guidance for direct laser writing of photonic structures in chalcogenide glasses.

Funding

National Natural Science Foundation of China (11674178, 61405241, 61475189); China Postdoctoral Science Foundation (2018M633603); K.C.Wong Education Foundation (GJTD-2018-08); Natural Science Basic Research Project in Shaanxi Province (2019JM-113, 2019JQ-236); Chinese Academy of Sciences Interdisciplinary Innovation Team Project.

References

1. J.-L. Adam and X. Zhang, *Chalcogenide Glasses: Preparation, Properties and Applications* (Woodhead Publishing, 2014).
2. S. D. Jackson, "Towards high-power mid-infrared emission from a fibre laser," Nat. Photonics **6**(7), 423–431 (2012).

Optical Materials EXPRESS

3. B. J. Eggleton, T. D. Vo, R. Pant, M. Pelusi, D. Yong Choi, S. Madden, and B. Luther-Davies, "Photonic chip based ultrafast optical processing based on high nonlinearity dispersion engineered chalcogenide waveguides," Laser Photonics Rev. **6**(1), 97–114 (2012).
4. M.-L. Anne, J. Keirsse, V. Nazabal, K. Hyodo, S. Inoue, C. Boussard-Pledel, H. Lhermite, J. Charrier, K. Yanakata, and O. Loreal, *et al.*, "Chalcogenide glass optical waveguides for infrared biosensing," Sensors **9**(9), 7398–7411 (2009).
5. S. Elliott, "AC conduction in amorphous chalcogenide and pnictide semiconductors," Adv. Phys. **36**(2), 135–217 (1987).
6. R. Frerichs, "New optical glasses with good transparency in the infrared," J. Opt. Soc. Am. **43**(12), 1153–1157 (1953).
7. G. Snopatin, V. Shiryaev, V. Plotnichenko, E. Dianov, and M. Churbanov, "High-purity chalcogenide glasses for fiber optics," Inorg. Mater. **45**(13), 1439–1460 (2009).
8. B. G. Aitken, C. W. Ponader, and R. S. Quimby, "Clustering of rare earths in GeAs sulfide glass," C. R. Chim. **5**(12), 865–872 (2002).
9. A. Galstyan, S. Messaddeq, V. Fortin, I. Skripachev, R. Vallée, T. Galstian, and Y. Messaddeq, "Tm^{3+} doped Ga–As–S chalcogenide glasses and fibers," Opt. Mater. **47**, 518–523 (2015).
10. A. B. Seddon, Z. Tang, D. Furniss, S. Sujecki, and T. M. Benson, "Progress in rare-earth-doped mid-infrared fiber lasers," Opt. Express **18**(25), 26704–26719 (2010).
11. J. Cui, X. Xiao, Y. Xu, X. Cui, M. Chen, J. Guo, M. Lu, B. Peng, and H. Guo, "Mid-infrared emissions of Dy $^{3+}$doped Ga-As-S chalcogenide glasses and fibers and their potential for a 4.2 μm fiber laser," Opt. Mater. Express **8**(8), 2089–2102 (2018).
12. X. H. Zhang, H. Ma, and J. Lucas, "Evaluation of glass fibers from the Ga–Ge–Sb–Se system for infrared applications," Opt. Mater. **25**(1), 85–89 (2004).
13. E. M. Dianov, I. Bufetov, A. A. Frolov, V. G. Plotnichenko, V. M. Mashinsky, M. F. Churbanov, and G. E. Snopatin, "Catastrophic destruction of optical fibres of various composition caused by laser radiation," Quantum Electron. **32**(6), 476–478 (2002).
14. C. You, S. Dai, P. Zhang, Y. Xu, Y. Wang, D. Xu, and R. Wang, "Mid-infrared femtosecond laser-induced damages in $As_2 S_3$ and $As_2 Se_3$ chalcogenide glasses," Sci. Rep. **7**(1), 6497 (2017).
15. S. Messaddeq, J. Bérubé, M. Bernier, I. Skripachev, R. Vallée, and Y. Messaddeq, "Study of the photosensitivity of GeS binary glasses to 800 nm femtosecond pulses," Opt. Express **20**(3), 2824–2831 (2012).
16. L. Petit, N. Carlie, T. Anderson, M. Couzi, J. Choi, M. Richardson, and K. Richardson, "Effect of IR femtosecond laser irradiation on the structure of new sulfo-selenide glasses," Opt. Mater. **29**(8), 1075–1083 (2007).
17. P. Knotek, J. Navesnik, T. Cernohorsky, M. Kincl, M. Vlcek, and L. Tichy, "Ablation of $(GeS_2)0.3(Sb_2S_3)$ 0.7 glass with an ultra-violet nano-second laser," Mater. Res. Bull. **64**, 42–50 (2015).
18. J. David Musgraves, N. Carlie, L. Petit, G. Boudebs, J. Choi, M. Richardson, and K. Richardson, "Effect of replacement of As by Ge and Sb on the photo-response under near infrared femtosecond laser irradiation in as-based sulfide glasses," Int. J. Appl. Glass Sci. **2**(4), 308–320 (2011).
19. Y. Zhang, Y. Xu, C. You, D. Xu, J. Tang, P. Zhang, and S. Dai, "Raman gain and femtosecond laser induced damage of Ge-As-S chalcogenide glasses," Opt. Express **25**(8), 8886–8895 (2017).
20. M. Zhang, T. Li, Y. Yang, H. Tao, X. Zhang, X. Yuan, and Z. Yang, "Femtosecond laser induced damage on Ge-As-S chalcogenide glasses," Opt. Mater. Express **9**(2), 555–561 (2019).
21. W. Rudulph and L. A. Emmert, "Laser-Induced Damage in Optical Materials," Encyclopedia of Modern Optics **4**, 302–309 (2018).
22. A. Miotello and R. Kelly, "Laser-induced phase explosion: new physical problems when a condensed phase approaches the thermodynamic critical temperature," Appl. Phys. A **69**(S1), S67–S73 (1999).
23. M. Asobe, T. Ohara, I. Yokohama, and T. Kaino, "Fabrication of Bragg grating in chalcogenide glass fibre using the transverse holographic method," Electron. Lett. **32**(17), 1611–1613 (1996).
24. M. Bernier, M. El-Amraoui, J. Couillard, Y. Messaddeq, and R. Vallée, "Writing of bragg gratings through the polymer jacket of low-loss as 2 s 3 fibers using femtosecond pulses at 800 nm," Opt. Lett. **37**(18), 3900–3902 (2012).
25. J. Liu, "Simple technique for measurements of pulsed gaussian-beam spot sizes," Opt. Lett. **7**(5), 196–198 (1982).
26. N. Bulgakova, A. Panchenko, V. Zhukov, S. Kudryashov, A. Pereira, W. Marine, T. Mocek, and A. Bulgakov, "Impacts of ambient and ablation plasmas on short-and ultrashort-pulse laser processing of surfaces," Micromachines **5**(4), 1344–1372 (2014).
27. I. Mirza, N. M. Bulgakova, J. Tomáštík, V. Michálek, O. Haderka, L. Fekete, and T. Mocek, "Ultrashort pulse laser ablation of dielectrics: Thresholds, mechanisms, role of breakdown," Sci. Rep. **6**(1), 39133 (2016).
28. J. Tauc, "Optical properties and electronic structure of amorphous semiconductors," Optical Properties of Solids, (Springer, 1969), pp. 123–136.
29. L. V. Keldysh, "On the theory of impact ionization in semiconductors," Sov. Phys, JETP **37**, 6 (1965).
30. E. Kamitsos, J. Kapoutsis, I. Culeac, and M. Iovu, "Structure and bonding in as- sb- s chalcogenide glasses by infrared reflectance spectroscopy," J. Phys. Chem. B **101**(51), 11061–11067 (1997).
31. A. Bertoluzza, C. Fagnano, P. Monti, and G. Semerano, "Raman and infrared spectra of As_2s_x chalcogenide glasses with x less than or equal to 3," J. Non-Cryst. Solids **29**(1), 49–60 (1978).

Optical Materials EXPRESS

32. M. Frumar, Z. Polak, and Z. Černošek, "Raman spectra and photostructural changes in the short-range order of amorphous as–s chalcogenides," J. Non-Cryst. Solids **256-257**, 105–110 (1999).
33. M. Kincl and L. Tichy, "Some Physical Properties of $Ge_xAs_xS_{1-2x}$ Glasses," Mater. Chem. Phys. **103**(1), 78–88 (2007).
34. J. Heo, J. M. Yoon, and S.-Y. Ryou, "Raman spectroscopic analysis on the solubility mechanism of La_3+ in GeS_2–Ga_2s_3 glasses," J. Non-Cryst. Solids **238**(1-2), 115–123 (1998).
35. L. Petit, N. Carlie, and F. Adamietz, "Correlation between physical, optical and structural properties of sulfide glasses in the system Ge-Sb-S," Mater. Chem. Phys. **97**(1), 64–70 (2006).
36. A. Yang, M. Zhang, L. Li, Y. Wang, B. Zhang, Z. Yang, and D. Tang, "Ga–sb–s chalcogenide glasses for mid-infrared applications," J. Am. Ceram. Soc. **99**(1), 12–15 (2016).
37. S. Emura, S.-I. Gonda, Y. Matsui, and H. Hayashi, "Internal-stress effects on raman spectra of InxGa1- x As on InP," Phys. Rev. B **38**(5), 3280–3286 (1988).
38. C. Hodgman, Handbook of chemistry and Physics (CRC Press, 1924).
39. C. Schaffer, J. Garćıa, and E. Mazur, "Bulk heating of transparent materials using a high-repetition-rate femtosecond laser," Appl. Phys. A: Mater. Sci. Process. **76**(3), 351–354 (2003).
40. C. Yang, M. Paesler, and D. Sayers, "Measurement of local structural configurations associated with reversible photostructural changes in arsenic trisulfide films," Phys. Rev. B **36**(17), 9160–9167 (1987).
41. O. Efimov, L. Glebov, K. Richardson, E. Van Stryland, T. Cardinal, S. H. Park, M. Couzi, and J. Bruneel, "Waveguide writing in chalcogenide glasses by a train of femtosecond laser pulses," Opt. Mater. **17**(3), 379–386 (2001).
42. G. Pfeiffer, M. Paesler, and S. Agarwal, "Reversible photodarkening of amorphous arsenic chalcogens," J. Non-Cryst. Solids **130**(2), 111–143 (1991).
43. P. Krecmer, M. Vlcek, and S. Elliott, "Novel photoinduced anisotropy in amorphous As50Se50 films at near the glass transition temperature," J. Non-Cryst. Solids **227-230**, 682–687 (1998).
44. A. K. Mairaj, P. Hua, H. N. Rutt, and D. W. Hewak, "Fabrication and characterization of continuous wave direct UV ($\lambda = 244^{-}$ nm) written channel waveguides in chalcogenide (Ga: La: S) glass," J. Lightwave Technol. **20**(8), 1578–1584 (2002).
45. H. A. Kramers, Collected Scientific Papers (North-Holland, 1956).
46. R. Rangel-Rojo, T. Kosa, E. Hajto, P. Ewen, A. Owen, A. Kar, and B. Wherrett, "Near-infrared optical nonlinearities in amorphous chalcogenides," Opt. Commun. **109**(1-2), 145–150 (1994).
47. K. Cerqua-Richardson, J. McKinley, B. Lawrence, S. Joshi, and A. Villeneuve, "Comparison of nonlinear optical properties of sulfide glasses in bulk and thin film form," Opt. Mater. **10**(2), 155–159 (1998).
48. J. Jasapara, A. Nampoothiri, W. Rudolph, D. Ristau, and K. Starke, "Femtosecond laser pulse induced breakdown in dielectric thin films," Phys. Rev. B **63**(4), 045117 (2001).
49. C. B. Schaffer, A. Brodeur, and E. Mazur, "Laser-induced breakdown and damage in bulk transparent materials induced by tightly focused femtosecond laser pulses," Meas. Sci. Technol. **12**(11), 1784–1794 (2001).
50. S. Irimiciuc, R. Boidin, G. Bulai, S. Gurlui, P. Nemec, V. Nazabal, and C. Focsa, "Laser ablation of $(GeSe_2)_{100-x}$ (Sb_2Se_3)x chalcogenide glasses: Influence of the target composition on the plasma plume dynamics," Appl. Surf. Sci. **418**(SI), 594–600 (2017).